ACS APPLIED BIO MATERIALS

www.acsabm.org

Article

Changes in the Secondary Structure and Assembly of Proteins on Fluoride Ceramic (CeF_3) Nanoparticle Surfaces

Naoya Sakaguchi, Samal Kaumbekova, Ryodai Itano, Mehdi Amouei Torkmahalleh, Dhawal Shah, and Masakazu Umezawa*

Cite This: *ACS Appl. Bio Mater.* 2022, 5, 2843−2850

Read Online

ACCESS | Metrics & More | Article Recommendations

ABSTRACT: Fluoride nanoparticles (NPs) are materials utilized in the biomedical field for applications including imaging of the brain. Their interactions with biological systems and molecules are being investigated, but the mechanism underlying these interactions remains unclear. We focused on possible changes in the secondary structure and aggregation state of proteins on the surface of NPs and investigated the principle underlying the changes using the amyloid β peptide ($A\beta_{16-20}$) based on infrared spectrometry. CeF_3 NPs (diameter 80 nm) were synthesized via thermal decomposition. Infrared spectrometry showed that the presence of CeF_3 NPs promotes the formation of the β-sheet structure of $A\beta_{16-20}$. This phenomenon was attributed to the hydrophobic interaction between NPs and Aβ peptides in aqueous environments, which causes the Aβ peptides to approach each other on the NP surface and form ordered hydrogen bonds. Because of the coexisting salts on the secondary structure and assembly of Aβ peptides, the formation of the β-sheet structure of Aβ peptides on the NP surface was suppressed in the presence of NH_4^+ and NO_3^- ions, suggesting the possibility that Aβ peptides were adsorbed and bound to the NP surface. The formation of the β-sheet structure of Aβ peptides was promoted in the presence of NH_4^+, whereas it was suppressed in the presence of NO_3^- because of the electrostatic interaction between the lysine residue of the Aβ peptide and the ions. Our findings will contribute to comparative studies on the effect of different NPs with different physicochemical properties on the molecular state of proteins.

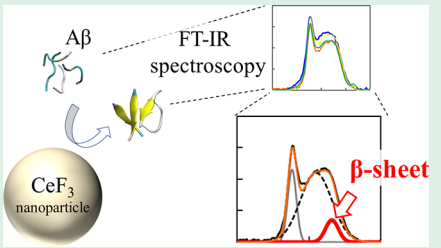

KEYWORDS: *amyloid β peptide, fluoride nanoparticles, infrared spectrometry, molecular dynamics, β-sheet*

INTRODUCTION

In the field of material sciences, the self-assembly of molecules is a major area of interest for researchers to develop soft matter.[1] Furthermore, in biology, the secondary structure and assembly state of a protein are important for regulating the function and activity of the protein. The formation of fibrillar aggregates of peptides and proteins is associated with various diseases including neurogenerative disorders.[2] The dysregulation of the structure and state of proteins can lead to diseases in biological organs.[3,4] For example, fibril formation via the self-assembly of denatured proteins causes amyloid diseases, such as Alzheimer's disease,[5] which is the most common neurodegenerative disease and is associated with cognitive and physical decline.[6] Pathologically, in patients with Alzheimer's diseases, senile (neuritic) plaques of the amyloid beta (Aβ) protein are observed in the brain tissue.[7]

Amino acid residues in proteins interact with each other through hydrogen bonds, disulfide bonds, electrostatic interactions, and hydrophobic interactions; these interactions affect protein conformation. As the distance between peptides reduces due to protein aggregation, their secondary structure can change due to an increase in interactions among peptides, for example, an increase in the β-sheet structure via enhanced hydrogen bonds. Although Aβ generally aggregates more at higher concentrations, even at low concentrations, it forms a β-sheet structure that can promote self-assembly via aromatic interactions between phenylalanine residues.[8,9] Especially, the hydrophobic domain of Aβ—the region around residues 17−20, LVFF—is important for β-sheet formation.[10]

In general, changes in the secondary structure and protein aggregation can be enhanced at liquid−liquid and liquid−air interfaces, as observed through denaturation by surfactants. In addition to these interfaces, liquid−solid interfaces are also likely to be the sites for protein denaturation because the domains with high affinity for the solid are exposed to the molecular surface. Molecular dynamics (MD) simulations have suggested that the structural arrangement of Aβ attached to the surface of carbon nanotubes—an inorganic nanomaterial—changes with the radius of the nanotubes.[11] The rate of peptide aggregation on the solid−liquid interface is determined by the affinity (binding force) between the peptide and the solid

Received: March 16, 2022
Accepted: May 17, 2022
Published: June 2, 2022

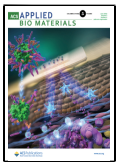

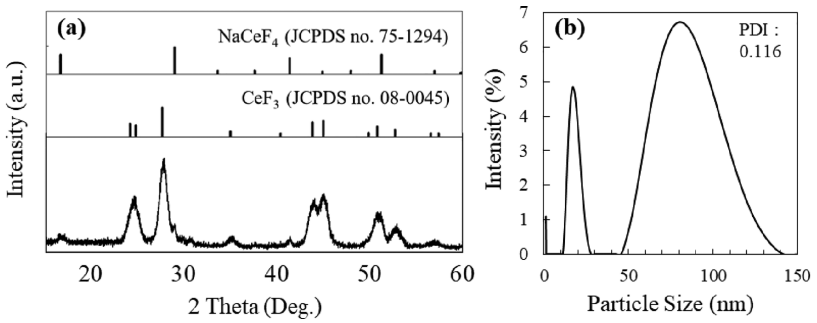

Figure 1. Characterization of fluoride NPs used in this study. (a) XRD pattern of the samples and references of CeF_3 (JCPDS no. 08-0045) and $NaCeF_4$ (JCPSD no. 75-1294). (b) DLS spectra showing the hydrodynamic diameter of the fluoride NPs dispersed in cyclohexane.

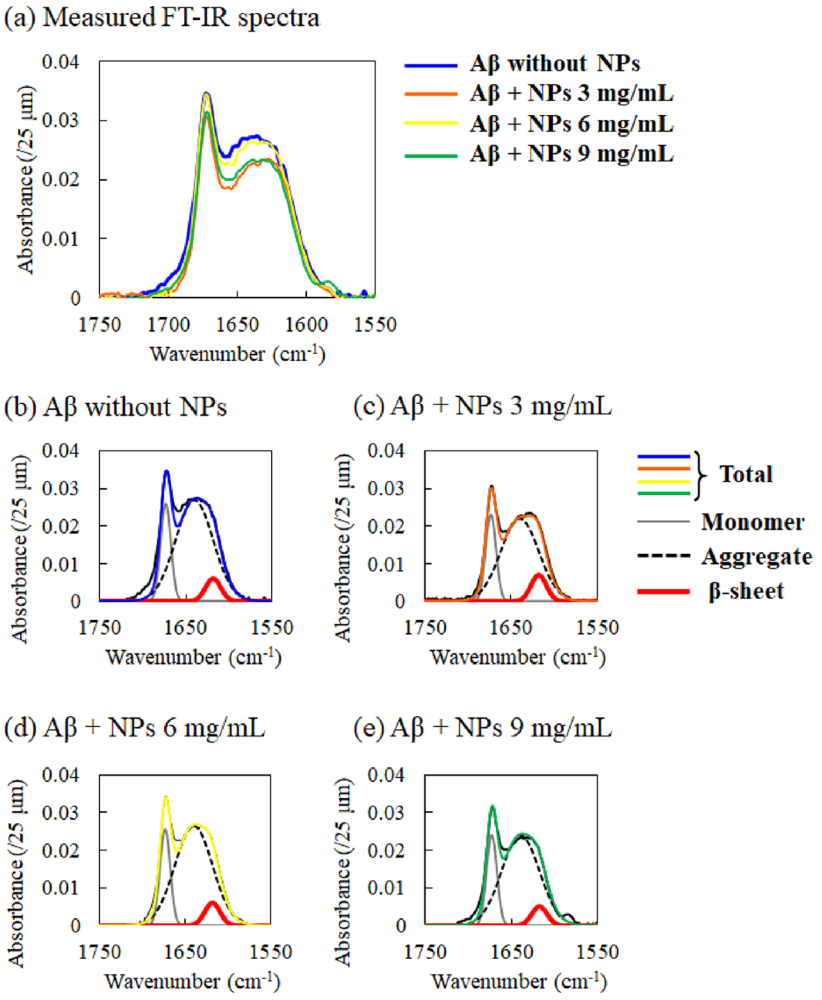

Figure 2. Amide I band in the FT-IR spectra of $A\beta_{16-20}$ interacted with CeF_3 NPs. (a) FT-IR spectra of $A\beta_{16-20}$ (6 mg/mL) that interacted with different concentrations of CeF_3 NPs (3, 6, and 9 mg/mL). (b−e) Deconvolution results via Gaussian fitting for the amide I band in FT-IR spectra of $A\beta_{16-20}$ (6 mg/mL) with CeF_3 NP concentrations of (b) 0, (c) 3, (d) 6, and (e) 9 mg/mL.

material and the shape (roughness) of the solid surface.[12] While a high affinity between peptides and solid surfaces enhances their adsorption and inhibits the self-assembly (aggregation) of peptides, solid materials with middle affinities and a rough surface (with a nanoscale morphology) accelerate the aggregation of peptides. In contrast, in a study in which all-atom MD simulations of the conformation of $A\beta_{16-22}$ peptides were performed, hydrophobic interactions were found to prevent the formation of β-sheet structures in the presence of gold nanoparticles (NPs).[13] The charge on the surface of NPs is also likely to be important for $A\beta$ fibrillation. Negatively charged NPs inhibit the formation of $A\beta$ fibrillation, whereas positively charged NPs have no effect on fibril formation.[14] The aggregation dynamics of $A\beta$ peptides ($A\beta_{16-21}$) on fullerene NP models was also investigated using MD simulation along with the effect of the coexistence of ionic salts.[15] However, there has still been no experimental evidence of how $A\beta$ peptides behave on NP surfaces in physiological environments containing salts.

https://doi.org/10.1021/acsabm.2c00239
ACS Appl. Bio Mater. 2022, 5, 2843−2850

In the present study, fluoride ceramic NPs, which are expected to be applied to the biomedical field, were used as a target material. Fluoride has a moderate phonon energy of 350 cm^{-1} and has been widely utilized in the biomedical field for applications such as brain imaging[16−18] as a fluorescent contrast agent containing rare-earth ions.[19−22] This is because it has both high chemical durability, as a lower phonon energy reduces the chemical stability similarly to chlorides, and high luminescence efficiency when doped with rare earths because higher phonon energy causes quenching via enhanced thermal relaxation.[23] Fluoride nanomaterials labeled within the long-wavelength (>1000 nm) near-infrared (NIR) region, called the second and third NIR (NIR-II/III) biological windows,[24] have been developed for NIR fluorescence computed tomography,[25] photodynamic therapy,[26] and fluorescence nanothermometers[27,28] for in vivo investigations of deep tissues such as tissues in the peritoneal cavity.[29] Rare-earth-doped fluoride crystals have also been developed for application in lifetime-based NIR fluorescence thermometers.[30] Fluoride crystals containing Gd^{3+} (e.g., $NaGdF_4$) and luminescent rare earths have been developed for bimodal imaging in fluorescence and magnetic resonance modalities.[31−36] CeF_3 NPs were used in this study as a fluoride ceramic that can show a surface reactivity similar to that of the fluorides, as mentioned above. The aim of this study was to investigate the effect of fluoride ceramic NPs, which are expected to have further biomedical applications, on the conformation and assembly of Aβ molecules using an in vitro experimental system and MD simulation.

RESULTS AND DISCUSSION

Fluoride NPs synthesized in this study were characterized using X-ray diffraction (XRD) and dynamic light scattering (DLS). As shown in Figure 1a, the XRD patterns showed that the NPs were majorly CeF_3 with small amounts of $NaCeF_4$. Data from DLS showed that the CeF_3 NPs showed a major peak at a diameter of 80 nm with a low polydispersity index (0.116), although it contained a minor fraction peak at 20 nm. We considered the representative CeF_3 particle size to be 80 nm of the peak in the size distribution in our following investigations.

In this study, fragment peptides with small molecular weights, Aβ_{16-20}, which allow MD simulations to be performed easily, were used to investigate the secondary conformational changes and aggregation of Aβ using both Fourier transform infrared (FT-IR) spectroscopy and the MD simulations. CeF_3 NPs were dispersed in an aqueous solution to interact with Aβ_{16-20} (KLVFF) in the aqueous solution. FT-IR spectroscopy was used for analyzing the secondary structure of proteins. Especially, the amide I vibration peak (appearing around 1650 cm^{-1} and mainly attributed to C═O stretching) was focused because it is hardly affected by the nature of the side chains but depends on the secondary structure of the backbone.[37] Thus, it is commonly used for the secondary structure analysis[38] that can also be applied to in situ analyses under microscopy.[39] Not only the secondary structure but also the aggregation of the Aβ peptide in solvents can be analyzed using FT-IR spectroscopy.[40] Hydrochloric acid (1 mmol/L) was used to maintain the dispersibility of the CeF_3 NPs. However, the water molecule showed peaks not only at 3300 cm^{-1} but also at 1650 cm^{-1} in the IR region; these peaks interfere with those of the amide I band at 1650 cm^{-1},[9] which is the target of analysis in this study. Therefore, deuterium chloride and deuterium oxide were used, instead of hydrochloric acid and water, as the dispersion media for CeF_3 and solution of Aβ_{16-20}. Deuterium chloride did not affect the FT-IR spectra of Aβ_{16-20} solution at this concentration (final 0.25 mmol/L) (data not shown). FT-IR spectra of the samples in which Aβ_{16-20} was interacted with different concentrations of CeF_3 NPs were analyzed. As shown in Figure 2a, Aβ_{16-20} showed two major peaks at 1674 and 1640 cm^{-1}, which correspond to aggregates and monomers, respectively.[9] Deconvolution analysis using Gaussian fitting showed that the FT-IR absorption spectra of Aβ_{16-20} also included, in addition to the major peaks, a minor peak at 1618 cm^{-1} corresponding to β-sheet formation of Aβ_{16-20}[9,38] (Figure 2b). The β-sheet formation of Aβ_{16-20} (6 mg/mL) increased in the presence of 3 mg/mL CeF_3 NPs, and this increase was not observed in the presence of 6 mg/mL CeF_3 NPs as the ratios of the β-sheet peak in the total amide I absorption were 6.8, 9.3, 6.9, and 6.3% in Aβ_{16-20} that interacted with 0, 3, 6, and 9 mg/mL of CeF_3 NPs, respectively (Figure 2b−e and Table 1). This may be due to the difference in the number of Aβ molecules per surface area of the NPs, which is the site of the NP−protein interaction in the system. Because the shape of CeF_3 NPs (density: 6.16 g/cm^3) is approximated to be a sphere with a diameter of 80 nm (2.7×10^5 nm^3/particle), the mass and surface area are 1.7×10^{-15} g and 2.0×10^4 nm,[2] respectively, leading to a specific surface area per mass of 1.2×10^{19} nm^2/g. The surface area of the CeF_3 particles in a dispersion of 3 mg/mL was 3.7×10^{16} nm^2/mL, while the total particle surface area in the dispersion was proportional to the particle concentration. Although the ratio of Aβ molecules that were attracted to the NP surface, that is, their local enrichment rate on the surface, in the dispersion was unknown, our results suggest that a certain enrichment of Aβ molecules promotes intermolecular bonding, thereby promoting β-sheet formation.

Table 1. Ratio of Each Component in the Amide I Band of the FT-IR Spectra of Aβ_{16-20} (6 mg/mL) That Interacted with Different Concentrations of CeF_3 NPs[a]

	Aβ	Aβ + NPs 3 mg/mL	Aβ + NPs 6 mg/mL	Aβ + NPs 9 mg/mL
monomer	0.20	0.20	0.20	0.20
aggregate	0.74	0.70	0.74	0.73
β sheet	0.068	0.093	0.069	0.063

[a]The ratios were obtained via deconvolution of the amide I band observed in each sample.

The effect of coexisting ions on the behavior of the Aβ_{16-20} peptide on the surface of CeF_3 NPs was studied using Aβ_{16-20} in D_2O with dissolved NaCl, NH_4Cl, and $NaNO_3$ (0.15 M). The effects of these ions at the same concentration were investigated in this experiment to compare the principle of action of each ion. Even without CeF_3 NPs, NH_4^+ promoted β-sheet formation of Aβ_{16-20}, whereas NO_3^- enhanced the monomer retention of Aβ_{16-20} (Table 2). Na^+ and Cl^- did not

Table 2. Ratio of Each Component in the Amide I Band of the FT-IR Spectra of Aβ_{16-20} (6 mg/mL) without and with Salts (0.15 M)

	Aβ	Aβ + NaCl	Aβ + NH_4Cl	Aβ + $NaNO_3$
monomer	0.21	0.21	0.19	0.23
aggregate	0.72	0.73	0.74	0.71
β sheet	0.067	0.062	0.075	0.057

https://doi.org/10.1021/acsabm.2c00239
ACS Appl. Bio Mater. 2022, 5, 2843−2850

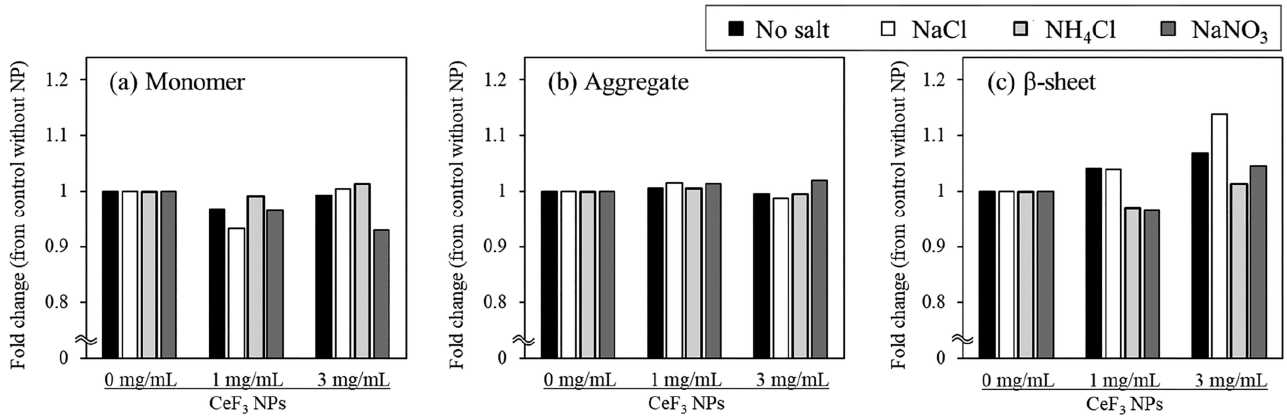

Figure 3. Increase in each separated peak (fold-change) in the amide I band of Aβ_{16-20} dissolved with salts due to CeF_3 NPs. The fold changes of the peaks of the (a) monomer (1674 cm^{-1}), (b) aggregate (1640 cm^{-1}), and (c) β-sheet (1618 cm^{-1}) of Aβ_{16-20} (6 mg/mL) dissolved in D_2O containing each salt (0.15 M) due to the coexistence of CeF_3 NPs (1 and 3 mg/mL) are shown.

Table 3. Average Distances (in nm) between the Centers of Mass of the Salt Ions and Aβ_{16-20} Peptide Residues at the End of the Simulation

	NaCl		NH_4Cl		$NaNO_3$	
peptide residue	Na^+	Cl^-	NH_4^+	Cl^-	Na^+	NO_3^-
K-16	1.21 ± 0.30	0.77 ± 0.20	1.25 ± 0.32	0.76 ± 0.23	0.95 ± 0.28	0.40 ± 0.03
L-17	1.13 ± 0.29	0.93 ± 0.21	1.30 ± 0.34	1.01 ± 0.24	1.06 ± 0.22	0.67 ± 0.08
V-18	1.30 ± 0.30	1.05 ± 0.23	1.31 ± 0.33	1.11 ± 0.22	1.09 ± 0.23	0.58 ± 0.04
F-19	1.31 ± 0.30	1.02 ± 0.23	1.20 ± 0.32	1.16 ± 0.26	1.08 ± 0.26	0.88 ± 0.14
F-20	1.14 ± 0.29	0.96 ± 0.22	1.11 ± 0.35	1.06 ± 0.30	0.97 ± 0.23	0.82 ± 0.17
average	1.22 ± 0.30	0.95 ± 0.24	1.23 ± 0.34	1.02 ± 0.29	1.03 ± 0.20	0.67 ± 0.20

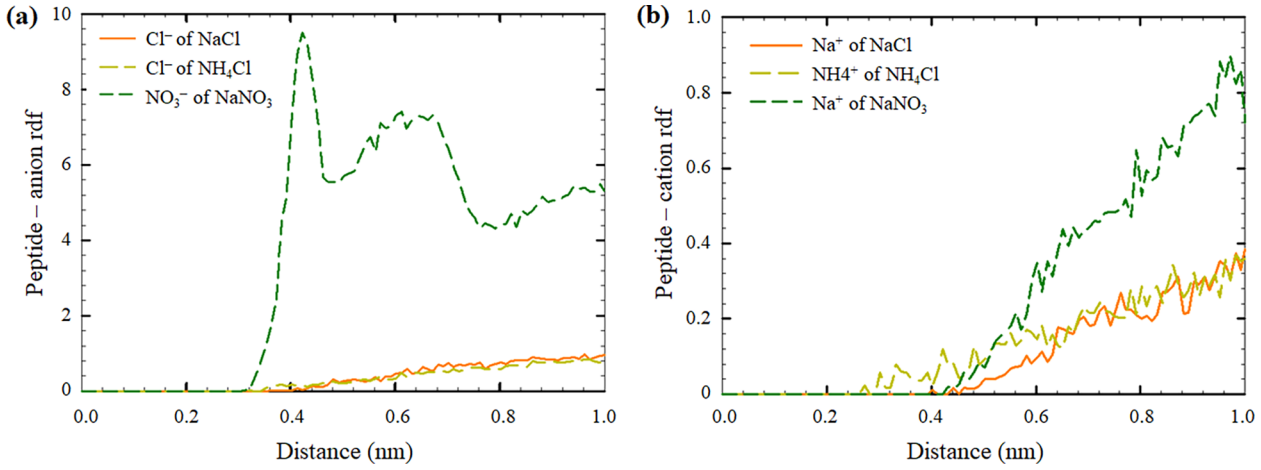

Figure 4. rdf plots of the interactions between Aβ_{16-20} peptides and the (a) anions and (b) cations. The results were averaged among four peptides present in the systems at the end of the MD simulations, when the systems were stabilized (last 10 ns of the MD run).

affect the amide I band of Aβ_{16-20} solution in D_2O (Table 2). β-Sheet formation of Aβ_{16-20} (6 mg/mL) was increased (14%) by CeF_3 NPs (3 mg/mL) in the presence of NaCl as well as in the absence of salts, whereas no elevation of β-sheet formation by NPs was observed in the presence of NH_4^+ and NO_3^- (Figure 3). The results suggest that NH_4^+ and NO_3^- suppressed the β-sheet formation of Aβ promoted on CeF_3. MD simulations were further performed on four monomers of Aβ_{16-20} in the presence of these salts. The findings showed that the NO_3^- was strongly bound to the peptide as compared to chloride in the absence of NPs. The average distance between the peptide and NO_3^- was 0.67 nm, whereas the distance with Cl^- was 0.99 nm (Table 3). Elevated peaks were observed on the radial distribution function (rdf) plots between peptide residues and NO_3^- and Na^+ of $NaNO_3$ with maximum peak values of ~9.5 at a 0.42 nm distance, as shown in Figure 4a, and ~0.88 at a 0.97 nm distance, as shown in Figure 4b). In contrast, comparatively low peak values were observed between peptides and ions of NaCl and NH_4Cl (with maximum peak values of ~0.96 at a 0.95 nm distance, as shown in Figure 4a, and ~0.38 at a 1.0 nm distance, as shown in Figure 4b), indicating their weak interactions. Among the different residues of Aβ_{16-20} (KLVFF), NO_3^- strongly interacted with the lysine (K-16) residue, with the average distance between lysine and NO_3^- being 0.4 nm (Table 3). The possible reasons for lysine and NO_3^- interactions are as

https://doi.org/10.1021/acsabm.2c00239
ACS Appl. Bio Mater. 2022, 5, 2843−2850

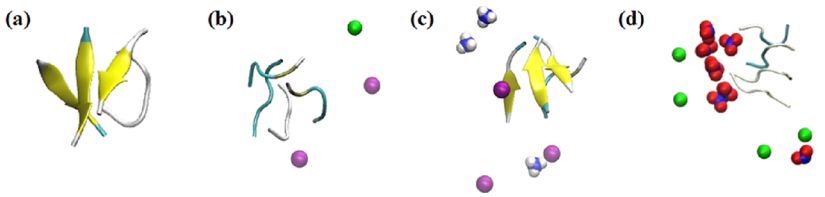

Figure 5. Representative snapshots of the peptide aggregates and ions within 0.1 nm of peptides in the systems under study: (a) no salt, (b) 0.15 M NaCl, (c) 0.15 M NH_4Cl, and (d) 0.15 M $NaNO_3$. Coloring methods in VMD: 1. Secondary structure of the peptide: beta sheet = yellow, beta bridge = tan, bend = cyan, turn = cyan, and coil = white. 2. Ions: Na^+ = green, NH_4^+ = blue and white, Cl^- = purple, and NO_3^- = blue and red.

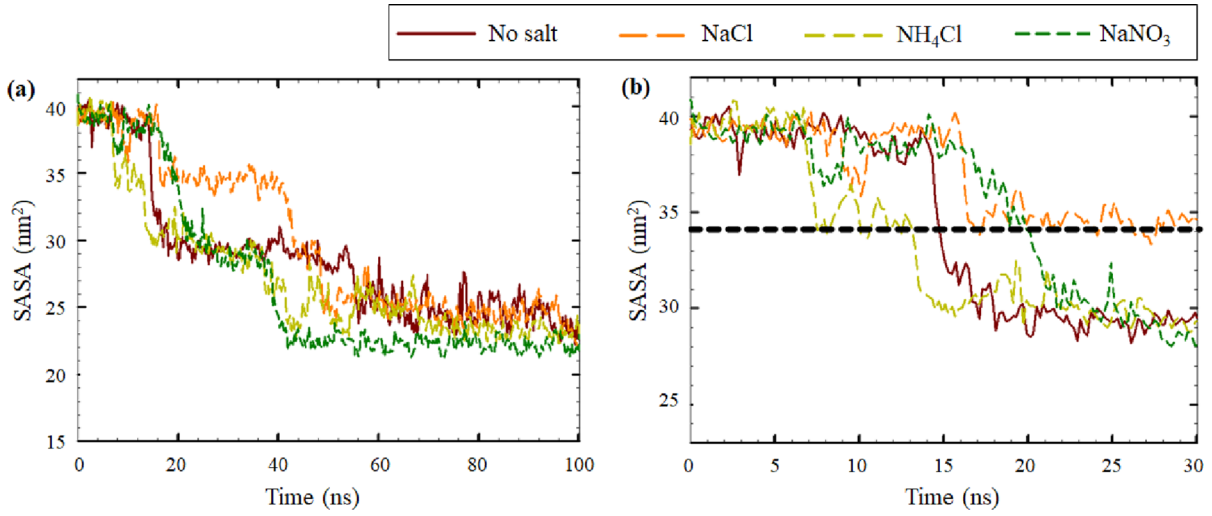

Figure 6. Time evolution of the total SASA of the Aβ_{16-20} peptides in the systems under study: (a) within 100 ns of the MD run and (b) within 30 ns of the MD run. The average values of each 200 ps of the simulation run were plotted, which corresponded to 50 frames of the run.

follows: 1) the strong electrostatic interactions between positively charged lysine and anions and 2) the formation of hydrogen bonds between lysine's sidechain and NO_3^-.[41] Consequently, these strong interactions suppressed the formation of β-sheets in the secondary structures of Aβ_{16-20} peptides in the $NaNO_3$ environment. Representative snapshots of the systems under study are shown in Figure 5. In addition to $NaNO_3$, as shown in Figure 4b and Table 3, the cation of NH_4Cl interacted with the phenylalanine (F) residues of Aβ_{16-20} via cation$-\pi$ interactions, which might have enhanced the β-sheet formation.[42]

The solvent accessible surface areas (SASAs) of the peptides were further studied to compare the aggregation kinetics under different environments (Figure 6). The total SASA ($SASA_0$) of the four peptides in the beginning of the simulation was 39 nm^2, which during the 100 ns of the simulations, decreased to ~22 nm^2 ($SASA_{100}$), indicating peptide aggregation (Figure 6a). The initial aggregation kinetics was quantified by estimating the time when the total SASA of peptides reached 34 nm^2 ($SASA_{34}$) during the first 30 ns of the simulations (Figure 6b). According to SASA plots (Figure 6b), enhanced aggregation kinetics was observed in the presence of 0.15 M NH_4Cl ($SASA_{34}$ was reached in 8 ns), which was related to the enhanced formation of beta sheets, observed from IR spectra (as shown previously in Table 2). The slowest aggregation kinetics was observed in the system with 0.15 M $NaNO_3$ ($SASA_{34}$ was reached in 19 ns), which corresponded to the retention of monomers in this environment, consistent with the results of IR absorption (shown previously on Table 2).

CONCLUSIONS

We evaluated the changes in the secondary structure and assembly of the Aβ peptide (Aβ_{16-20}) due to CeF_3 NPs using liquid film FT-IR measurements and MD simulations. CeF_3 NPs were found to locally concentrate Aβ_{16-20} on their surfaces, possibly due to the hydrophobic interaction between NPs and Aβ_{16-20} in aqueous environments, and promote the β-sheet formation of Aβ_{16-20}. The concentrated Aβ_{16-20} on the NP surface formed ordered hydrogen bonds to form a β-sheet. This increase in the β-sheet formation of Aβ_{16-20} on the NP surfaces was suppressed in the presence of NH_4^+ and NO_3^- ions. Hydrogen bonding between Aβ peptides were dominant when concentrated on CeF_3 NP surfaces in the absence of NH_4^+ or NO_3^-. In the presence of NH_4^+ or NO_3^-, the hydrogen bonding was suppressed due to dominant bonding between the NPs and Aβ peptides. The formation of the β-sheet structure of Aβ peptides was promoted in the presence of NH_4^+ ions, whereas it was suppressed in the presence of NO_3^- ions regardless of the presence/absence of CeF_3 NPs, which can be explained by the electrostatic interaction between the lysine residue (amino group) of Aβ peptides and the ions. Although this study was performed using the Aβ_{16-20} peptide, future research will be conducted using full-length Aβ (Aβ_{1-42}) to reveal more realistic in vivo phenomena. The analysis technique using FT-IR spectroscopy and MD will contribute to comparative studies of the effect of NPs on the molecular state of proteins under various physicochemical conditions.

MATERIALS AND METHODS

Materials. Cerium (III) chloride heptahydrate ($CeCl_3 \cdot 7H_2O$), oleic acid, deuterium oxide (D_2O), and amyloid beta (16−20)

https://doi.org/10.1021/acsabm.2c00239
ACS Appl. Bio Mater. 2022, 5, 2843−2850

peptide [Aβ_{16-20}; Ac-Lys-(Me)Leu-Val-(Me)Phe-Phe-NH_2] were purchased from Sigma-Aldrich Co. (St Louis, MO, USA), and 1-octadecene was purchased from Tokyo Chemical Industry Co., Ltd. (Tokyo, Japan). The N-methylated form of Aβ_{16-20} is a commercially available good model for the investigation with increased stability; however, possible changes in the peptide conformation and aggregation state associated with a possible increase in hydrophobicity should be noted. Sodium hydroxide, ammonium chloride (NH_4Cl), sodium nitrate ($NaNO_3$), sodium chloride (NaCl), methanol, ethanol, hexane, cyclohexane, and 20% deuterium chloride solution (DCl) (5.34 mol/L) in D_2O were purchased from Fujifilm Wako Pure Chemical Co. (Osaka, Japan). Ammonium fluoride was purchased from Kanto Chemical Co., Inc. (Tokyo, Japan). All reagents were used without further purification.

Synthesis and Characterization of CeF_3 NPs. Fluoride NPs were synthesized via thermal decomposition.[43] $CeCl_3{\cdot}7H_2O$ (1 mmol) was dissolved in distilled water (3 mL), mixed with oleic acid (12 mL) and 1-octadecene (30 mL), and stirred at 100 °C for 20 min and at 160 °C for 40 min in a nitrogen atmosphere, giving cerium oleate. After cooling to 50 °C, sodium hydroxide (2.5 mmol) and ammonium fluoride (4 mmol) dissolved in methanol were slowly added to the cerium oleate sample, and the sample was heated at 100 °C for 20 min and further at 310 °C for 50 min in a nitrogen atmosphere. The NPs collected via precipitation were purified using centrifugal washing (20 000 g, 10 min, ×3) with a hexane−ethanol mixed solvent and dispersed in cyclohexane. The NPs were characterized using XRD (Rint-Ultima 3, Rigaku Co., Tokyo, Japan) and DLS (ELSZ-2000ZS, Otsuka Electronics Co., Ltd., Osaka, Japan).

FT-IR Spectroscopy for Samples in Solution. Fluoride NPs (27 mg/mL) in cyclohexane (750 μL) were slowly added dropwise into 1 mmol/L DCl solution in D_2O (750 μL) and stirred for 16 h to remove cyclohexane via evaporation and to exchange the dispersion media with DCl/D_2O. Aβ_{16-20} was dissolved in D_2O at 8 mg/mL. The Aβ_{16-20} solution (8 mg/mL) in D_2O with and without NH_4Cl, $NaNO_3$, or NaCl (0.2 M) was mixed with different concentrations (3−27 mg/mL) of the NP dispersion in 1 mmol/L DCl solution at a 3:1 volume ratio (thus, the final concentration of Aβ_{16-20} in the mixed samples was 6 mg/mL). The final concentrations of the NPs were set at 1−9 mg/mL because the concentration order of milligrams per milliliter is the dose commonly used for imaging contrast agents for visualizing blood flow.[27,36,44] FT-IR spectra including amide bands were recorded using an FT/IR-6200 spectrometer (Shimadzu Co., Kyoto, Japan) for the mixed samples sandwiched between two CaF_2 plate windows (spacer 0.025 mm). The analysis was performed for each sample within 30 min after mixing Aβ_{16-20} with the NP dispersion.

MD Simulations. MD simulations were performed using GROMACS 2019.6 software with a GROMOS 54A7 force field. Four Aβ_{16-20} peptide monomers with a concentration of 6 mg/mL were inserted in a 9 × 9 × 9 nm^3 box. The simulations were performed in the absence of salts and in the presence of 0.15 M NaCl, NH_4Cl, and $NaNO_3$ solutions. The MD run was performed for 100 ns for each system, following the methodology described in a previous study.[15]

Analysis of the MD Simulations. Formation of peptide aggregates and kinetics of aggregation were studied via SASA analysis. The interactions between ions and peptide residues were studied in the last 10 ns of the simulations, when the peptide aggregates were produced. The rdf and intermolecular distance analyses were performed using the centers of mass of the peptides, averaged among four peptides. Visual molecular dynamics (VMD) software was used for the visualization of the systems under the study.

AUTHOR INFORMATION

Corresponding Author

Masakazu Umezawa − *Department of Materials Science and Technology, Faculty of Advanced Engineering, Tokyo University of Science, Tokyo 125-8585, Japan;* orcid.org/0000-0002-3398-3993; Email: masa-ume@rs.tus.ac.jp

Authors

Naoya Sakaguchi − *Department of Materials Science and Technology, Faculty of Advanced Engineering, Tokyo University of Science, Tokyo 125-8585, Japan*

Samal Kaumbekova − *Department of Chemical and Materials Engineering, School of Engineering and Digital Sciences, Nazarbayev University, Nur-Sultan 010000, Kazakhstan;* orcid.org/0000-0001-6477-3916

Ryodai Itano − *Department of Materials Science and Technology, Faculty of Advanced Engineering, Tokyo University of Science, Tokyo 125-8585, Japan*

Mehdi Amouei Torkmahalleh − *Department of Chemical and Materials Engineering, School of Engineering and Digital Sciences, Nazarbayev University, Nur-Sultan 010000, Kazakhstan;* orcid.org/0000-0003-0092-1558

Dhawal Shah − *Department of Chemical and Materials Engineering, School of Engineering and Digital Sciences, Nazarbayev University, Nur-Sultan 010000, Kazakhstan;* orcid.org/0000-0002-0450-5001

Complete contact information is available at: https://pubs.acs.org/10.1021/acsabm.2c00239

Author Contributions

M.U. was the main project leader and conceived the overall research idea. N.S. performed the in vitro experiments, data collection, and analysis. N.S., R.I., and M.U. were substantially involved in the in vitro data analysis and interpretation. S.K. performed the MD analysis under supervision of M.A.T. and D.S. N.S. S.K., and M.U. drafted the manuscript and edited it with M.A.T. and D.S. All authors read and approved the final manuscript prior to submission.

Funding

Tokyo University of Science: Faculty of Advanced Engineering Young Scientist Collaborative Research grant (2021). Nazarbayev University: collaborative research project (11022021CRP1503).

Notes

The authors declare no competing financial interest.

ACKNOWLEDGMENTS

The authors thank Hiroyuki Kurahashi and Junsuke Katayama (Tokyo University of Science) for technical assistance with synthesis and characterization of CeF_3 NPs and Kotoe Ichihashi and Konosuke Sato for assistance with FT-IR spectral analysis. The authors would like to acknowledge the Faculty of Advanced Engineering of Tokyo University of Science for providing the financial resources for the in vitro experimental part of this study through a Young Scientist Collaborative Research grant (2021, M.U.) and Nazarbayev University for providing the financial resources for the MD part of this study through a collaborative research project (11022021CRP1503, M.A.T.).

REFERENCES

(1) Hamley, I. W.; Castelletto, V. Biological Soft Materials. *Angew. Chem., Int. Ed. Engl.* **2007**, *46*, 4442−4455.

(2) Chiti, F.; Dobson, C. M. Protein Misfolding, Functional Amyloid, and Human Disease. *Annu. Rev. Biochem.* **2006**, *75*, 333−366.

(3) Zerovnik, E. Amyloid-Fibril Formation. Proposed Mechanisms and Relevance to Conformational Disease. *Eur. J. Biochem.* **2002**, *269*, 3362−3371.
(4) Meredith, S. C. Protein Denaturation and Aggregation: Cellular Responses to Denatured and Aggregated Proteins. *Ann. N.Y. Acad. Sci.* **2005**, *1066*, 181−221.
(5) Goedert, M.; Spillantini, M. G. A Century of Alzheimer's Disease. *Science* **2006**, *314*, 777−781.
(6) Kepp, K. P. Bioinorganic Chemistry of Alzheimer's Disease. *Chem. Rev.* **2012**, *112*, 5193−5239.
(7) Murphy, M. P.; LeVine, H., III Alzheimer's Disease and the Amyloid-β Peptide. *J. Alzheimer's Dis.* **2010**, *19*, 311−323.
(8) Krysmann, M. J.; Castelletto, V.; Hamley, I. W. Fibrillisation of Hydrophobically Modified Amyloid Peptide Fragments in an Organic Solvent. *Soft Matter* **2007**, *3*, 1401−1406.
(9) Krysmann, M. J.; Castelletto, V.; Kelarakis, A.; Hamley, I. W.; Hule, R. A.; Pochan, D. J. Self-Assembly and Hydrogelation of an Amyloid Peptide Fragment. *Biochemistry* **2008**, *47*, 4597−4605.
(10) Hilbich, C.; Kisters-Woike, B.; Reed, J.; Masters, C. L.; Beyreuther, K. Substitutions of hydrophobic amino acids reduce the amyloidogenicity of Alzheimer's disease βA4 peptides. *J. Mol. Biol.* **1992**, *228*, 460−473.
(11) Xing, Y.; Sun, Y.; Wang, B.; Ding, F. Morphological Determinants of Carbon Nanomaterial-Induced Amyloid Peptide Self-Assembly. *Front. Chem.* **2020**, *8*, 160.
(12) Co, N.; Li, M. Effect of Surface Roughness on Aggregation of Polypeptide Chains: A Monte Carlo Study. *Biomolecules* **2021**, *11*, 596.
(13) Song, M.; Sun, Y.; Luo, Y.; Zhu, Y.; Liu, Y.; Li, H. Exploring the Mechanism of Inhibition of au Nanoparticles on the Aggregation of Amyloid-β(16-22) Peptides at the Atom Level by All-Atom Molecular Dynamics. *Int. J. Mol. Sci.* **2018**, *19*, 1815.
(14) Sudhakar, S.; Kalipillai, P.; Santhosh, P. B.; Mani, E. Role of Surface Charge of Inhibitors on Amyloid Beta Fibrillation. *J. Phys. Chem. C* **2017**, *121*, 6339−6348.
(15) Kaumbekova, S.; Torkmahalleh, M. A.; Shah, D. Impact of ultrafine particles and secondary inorganic ions on early onset and progression of amyloid aggregation: Insights from molecular simulations. *Environ. Pollut.* **2021**, *284*, 117147.
(16) Zhong, Y.; Ma, Z.; Zhu, S.; Yue, J.; Zhang, M.; Antaris, A. L.; Yuan, J.; Cui, R.; Wan, H.; Zhou, Y.; Wang, W.; Huang, N. F.; Luo, J.; Hu, Z.; Dai, H. Boosting the down-shifting luminescence of rare-earth nanocrystals for biological imaging beyond 1500 nm. *Nat. Commun.* **2017**, *8*, 737.
(17) Zhao, J.; Hu, H.; Liu, W.; Wang, X. Multifunctional $NaYF_4$:Nd/$NaDyF_4$ nanocrystals as a multimodal platform for NIR-II fluorescence and magnetic resonance imaging. *Nanoscale Adv.* **2021**, *3*, 463.
(18) Jiang, X.; Pu, R.; Wang, C.; Xu, J.; Tang, Y.; Qi, S.; Zhan, Q.; Wei, X.; Gu, B. Noninvasive and early diagnosis of acquired brain injury using fluorescence imaging in the NIR-II window. *Biomed. Opt. Express* **2021**, *12*, 6984.
(19) Nyk, M.; Kumar, R.; Ohulchanskyy, T. Y.; Bergey, E. J.; Prasad, P. N. High Contrast in Vitro and in Vivo Photoluminescence Bioimaging Using Near Infrared to Near Infrared Up-Conversion in Tm^{3+} and Yb^{3+} Doped Fluoride Nanophosphors. *Nano Lett.* **2008**, *8*, 3834−3838.
(20) Naczynski, D. J.; Tan, M. C.; Zevon, M.; Wall, B.; Kohl, J.; Kulesa, A.; Chen, S.; Roth, C. M.; Riman, R. E.; Moghe, P. V. Rare-Earth-Doped Biological Composites as in Vivo Shortwave Infrared Reporters. *Nat. Commun.* **2013**, *4*, 2199.
(21) Jaque, D.; Richard, C.; Viana, B.; Soga, K.; Liu, X.; García Solé, J. Inorganic Nanoparticles for Optical Bioimaging. *Adv. Opt. Photonics* **2016**, *8*, 1−103.
(22) Lei, X.; Li, R.; Tu, D.; Shang, X.; Liu, Y.; You, W.; Sun, C.; Zhang, F.; Chen, X. Intense Near-Infrared-II Luminescence from $NaCeF_4$:Er/Yb Nanoprobes for in Vitro Bioassay and in Vivo Bioimaging. *Chem. Sci.* **2018**, *9*, 4682−4688.
(23) Okubo, K.; Umezawa, M.; Soga, K. Review-Concept and Application of Thermal Phenomena at 4f Electrons of Trivalent Lanthanide Ions in Organic/Inorganic Hybrid Nanostructure. *ECS J. Solid State Sci. Technol.* **2021**, *10*, 096006.
(24) Smith, A. M.; Mancini, M. C.; Nie, S. Second window for in vivo imaging. *Nat. Nanotechnol.* **2009**, *4*, 710−711.
(25) Umezawa, M.; Sera, T.; Yokota, H.; Takematsu, M.; Morita, M.; Yeroslavsky, G.; Kamimura, M.; Soga, K. Computed Tomography for in Vivo Deep Over-1000 Nm Near-Infrared Fluorescence Imaging. *J. Biophotonics* **2020**, *13*, No. e20200071.
(26) Tezuka, K.; Umezawa, M.; Liu, T.-I.; Nomura, K.; Okubo, K.; Chiu, H.-C.; Kamimura, M.; Soga, K. Upconversion Luminescent Nanostructure with Ultrasmall Ceramic Nanoparticles Coupled with Rose Bengal for NIR-Induced Photodynamic Therapy. *ACS Appl. Bio Mater.* **2021**, *4*, 4462−4469.
(27) Kamimura, M.; Matsumoto, T.; Suyari, S.; Umezawa, M.; Soga, K. Ratiometric Near-Infrared Fluorescence Nanothermometry in the OTN-NIR (NIR II/III) Biological Window Based on Rare-Earth Doped β-$NaYF_4$ Nanoparticles. *J. Mater. Chem. B* **2017**, *5*, 1917−1925.
(28) Ximendes, E. C.; Pereira, A. F.; Rocha, U.; Silva, W. F.; Jaque, D.; Jacinto, C. Thulium Doped LaF_3 for Nanothermometry Operating over 1000 Nm. *Nanoscale* **2019**, *11*, 8864−8869.
(29) Sekiyama, S.; Umezawa, M.; Kuraoka, S.; Ube, T.; Kamimura, M.; Soga, K. Temperature sensing of deep abdominal region in mice by using over-1000 nm near-infrared luminescence of rare-earth-doped NaYF4 nanothermometer. *Sci. Rep.* **2018**, *8*, 16979.
(30) Chihara, T.; Umezawa, M.; Miyata, K.; Sekiyama, S.; Hosokawa, N.; Okubo, K.; Kamimura, M.; Soga, K. Biological deep temperature imaging with fluorescence lifetime of rare-earth-doped ceramics particles in the second NIR biological window. *Sci. Rep.* **2019**, *9*, 12806.
(31) Ma, D.; Xu, X.; Hu, M.; Wang, J.; Zhang, Z.; Yang, J.; Meng, L. Rare-Earth-Based Nanoparticles with Simultaneously Enhanced Near-Infrared (NIR)-Visible (Vis) and NIR-NIR Dual-Conversion Luminescence for Multimodal Imaging. *Chem.−Asian J.* **2016**, *11*, 1050−1058.
(32) Wang, P.; Wang, C.; Lu, L.; Li, X.; Wang, W.; Zhao, M.; Hu, L.; El-Toni, A. M.; Li, Q.; Zhang, F. Kinetics-Mediate Fabrication of Multi-Model Bioimaging Lanthanide Nanoplates with Controllable Surface Roughness for Blood Brain Barrier Transportation. *Biomaterials* **2017**, *141*, 223−232.
(33) Ma, L.; Liu, Y.; Liu, L.; Jiang, A.; Mao, F.; Liu, D.; Wang, L.; Zhou, J. Simultaneous Activation of Short-Wave Infrared (SWIR) Light and Paramagnetism by a Functionalized Shell for High Penetration and Spatial Resolution Theranostics. *Adv. Funct. Mater.* **2018**, *28*, 1705057.
(34) Ren, F.; Ding, L.; Liu, H.; Huang, Q.; Zhang, H.; Zhang, L.; Zeng, J.; Sun, Q.; Li, Z.; Gao, M. Ultra-Small Nanocluster Mediated Synthesis of Nd3+-Doped Core-Shell Nanocrystals with Emission in the Second Near-Infrared Window for Multimodal Imaging of Tumor Vasculature. *Biomaterials* **2018**, *175*, 30−43.
(35) Ren, Y.; He, S.; Huttad, L.; Chua, M.-S.; So, S. K.; Guo, Q.; Cheng, Z. An NIR-II/MR Dual Modal Nanoprobe for Liver Cancer Imaging. *Nanoscale* **2020**, *12*, 11510−11517.
(36) Okubo, K.; Takeda, R.; Murayama, S.; Umezawa, M.; Kamimura, M.; Osada, K.; Aoki, I.; Soga, K. Size-Controlled Bimodal in Vivo Nanoprobes as Near-Infrared Phosphors and Positive Contrast Agents for Magnetic Resonance Imaging. *Sci. Technol. Adv. Mater.* **2021**, *22*, 160−172.
(37) Jiang, Y.; Li, C.; Nguyen, X.; Muzammil, S.; Towers, E.; Gabrielson, J.; Narhi, L. Qualification of FTIR Spectroscopic Method for Protein Secondary Structural Analysis. *J. Pharm. Sci.* **2011**, *100*, 4631−4641.
(38) Barth, A.; Zscherp, C. What Vibrations Tell about Proteins. *Q. Rev. Biophys.* **2002**, *35*, 369−430.
(39) Onoda, A.; Kawasaki, T.; Tsukiyama, K.; Takeda, K.; Umezawa, M. Perivascular accumulation of β-sheet-rich proteins in offspring

https://doi.org/10.1021/acsabm.2c00239
ACS Appl. Bio Mater. 2022, 5, 2843−2850

brain following maternal exposure to carbon black nanoparticles. *Front. Cell. Neurosci.* **2017**, *11*, 92.
(40) Szabó, Z.; Jost, K.; Soós, K.; Zarándi, M.; Kiss, J. T.; Penke, B. Solvent Effect on Aggregational Properties of β-Amyloid Polypeptides Studied by FT−IR Spectroscopy. *J. Mol. Struct.* **1999**, *480*−*481*, 481−487.
(41) Song, X.; Hamano, H.; Minofar, B.; Kanzaki, R.; Fujii, K.; Kameda, Y.; Kohara, S.; Watanabe, M.; Ishiguro, S.-i.; Umebayashi, Y. Structural Heterogeneity and Unique Distorted Hydrogen Bonding in Primary Ammonium Nitrate Ionic Liquids Studied by High-Energy X-Ray Diffraction Experiments and MD Simulations. *J. Phys. Chem. B* **2012**, *116*, 2801−2813.
(42) Orabi, E. A.; Lamoureux, G. Cation-π Interactions between Quaternary Ammonium Ions and Amino Acid Aromatic Groups in Aqueous Solution. *J. Phys. Chem. B* **2018**, *122*, 2251−2260.
(43) Li, Z.; Zhang, Y. An efficient and user-friendly method for the synthesis of hexagonal-phase $NaYF_4$:Yb, Er/Tm nanocrystals with controllable shape and upconversion fluorescence. *Nanotechnology* **2008**, *19*, 345606.
(44) Ueya, Y.; Umezawa, M.; Takamoto, E.; Yoshida, M.; Kobayashi, H.; Kamimura, M.; Soga, K. Designing highly emissive over-1000-nm near-infrared fluorescent dye-loaded polystyrene-based nanoparticles for in vivo deep imaging. *RSC Adv.* **2021**, *11*, 18930−18937.

https://doi.org/10.1021/acsabm.2c00239
ACS Appl. Bio Mater. 2022, 5, 2843−2850